Study on low hydrostatic pressure-dependent optoelectronic and thermoelectric properties of lead-free perovskite $NaGeI_3$

Student ID: 181333
Session: 2018-2019

Report submitted to the Department of Physics at
Jashore University of Science and Technology
in partial fulfillment of the requirements
for the degree of Bachelor of Science
with Honours in Physics

January 2024

Abstract

The structural, electronic, optical, and thermoelectric properties of the Ge-based lead-free halide perovskite $NaGeI_3$ have been investigated under various hydrostatic pressures ranging from 0 to 4 GPa utilizing the self-consistent Full-Potential Linearized Augmented Plane-Wave (FP-LAPW) method based on density functional theory (DFT), as implemented in the WIEN2k package. According to the structural investigation, the optimized lattice constant for $NaGeI_3$ at 0 GPa is 5.91 Å, which reduces with applied pressure. Additionally, the studied perovskites have a direct bandgap of about 0.49 eV, indicating semiconducting behavior at ambient pressure. The bandgap decreases with an incremental application of pressure. Moreover, the optical functions improve under pressure, suggesting that these materials could be used in various optoelectronic devices operating in the visible and ultraviolet spectrums. The thermoelectric properties of the compound are explained in terms of electrical conductivity, thermal conductivity, Seebeck coefficient, figure of merit, and power factor. The study unveils promising properties of $NaGeI_3$ under different pressures, opening new avenues for its application in optoelectronic devices.

Acknowledgements

First of all, I praise and thank almighty Allah, the Lord of the worlds, the Most Merciful, the Guider of hearts, the Provider of sustenance, the Owner of life and death.

I would like to thank my supervisor, Dr. Mohammad Abdur Rashid, for his constant support and guidance to complete my project work properly. During the peroid of this project, he always shows me invaluable confidence. I appreciate all the faculty members of Department of Physics. I want to express my gratitude to the Quantum Materials Simulation Lab (QMSL) members who supported me throughout the project, both directly and indirectly. They taught me how to precisely calculate all characteristics and provided a wealth of knowledge that helped me produce an appropriate project report. They are helpful and amicable. Besides, I have got many facilities from QMSL, printing is one of them.

On a personal note, I would like to thank my respectable parents for their sacrifice and support over the years. Their love and encouragement always give me mental support to continue my study smoothly.

Contents

Study on low hydrostatic pressure-dependent optoelectronic and thermoelectric properties of lead-free perovskite $NaGeI_3$.

List of Figures

List of Tables

Study on low hydrostatic pressure-dependent optoelectronic and thermoelectric properties of lead-free perovskite $NaGeI_3$

Chapter 1

Introduction

In recent years, the increasing demand and the continuous decrease in natural energy resources has driven the scientific community to explore advanced devices for harvesting energy from natural sources [1, 2]. Currently, perovskite materials have gained significant attention among scientists due to their efficiency, remarkable adaptability, and the simplicity of their manufacturing processes [3,4]. Halide-based perovskites have recently witnessed a substantial upswing in solar cell device performance due to their application in solar photovoltaic systems [5–7]. In less than ten years, the energy conversion efficiency of perovskite solar cells has increased at a staggering rate, exceeding 25% [8–10]. Notably, perovskite solar cells have rapidly advanced in efficiency, while maintaining a cost-effective production process [11–13]. The ease of fabrication using simple, solution-based methods makes them highly scalable [14–16]. Perovskites excel in light absorption across a wide spectrum, making them exceptional at converting sunlight into electricity [17–19].

Perovskite compounds have a general formula of ABX_3, where A and B represent the cations, and X (oxygen or halogens) is an anion [20,21]. These generic varieties provide a broad range of compositions, enabling the fine-tuning of their characteristics for specific applications such as solar cells, LEDs, and sensors [22, 23]. Many researchers already have published their articles on perovskite materials. As example,

Introduction

Michael M Lee et al. report a low-cost, solution-processable solar cell, based on a highly crystalline perovskite absorber with intense visible to near-infrared absorptivity, that has a power conversion efficiency of 10.9% in a single-junction device under simulated full sunlight [24]. Rabia Sharif et al. and Arshi Khalid et al. represents a comprehensive review of the current progresses and material advances in perovskite solar cells [25]. They discussed the impact of layers such as ETLs and buffer-layers employed in perovskite solar-cells, seeing their transmittance, carrier mobility, and band gap potentials in commercialization. Mohammad Abdur Rashid et al. and Md Saiduzzaman et al. explored the changes in mechanical and optoelectronic behavior of semiconducting lead-free halide perovskites $RbSnX_3$ (X = Cl, Br) under uniform hydrostatic pressure for sustainable device applications [26]. Md Borhanul Asfia et al. and Sahadat Jaman et al. studied the pressure effect on $RbSrCl_3$ to see the band gap shifting properties for optoelectronic applications [27].

Nowadays, influence of pressure on perovskite compounds is a subject of intense research, revealing intriguing effects on both the structural and electronic characteristics of these materials [28–31]. Understanding the pressure-dependent behavior of perovskites is crucial for tailoring their properties to specific applications, ranging from optoelectronic devices to energy storage systems [32–34]. Under pressure, changes in the lattice parameters can be observed, impacting the arrangement of atoms within the crystal lattice [35]. Notably, alterations in the electronic band structure occur, influencing the electrical conductivity and optical properties of perovskites. The application of pressure may also induce phase transitions, leading to modifications in symmetry and overall crystal structure [36]. Researchers are actively exploring how these pressure-induced changes can enhance the functionalities of perovskite materials, opening up possibilities for improved performance in applications such as optoelectronic devices and energy storage systems.

In this work, we choose Ge-based lead-free perovskite halide $NaGeI_3$ under uniform hydrostatic pressures up to 4 GPa, to study the structural, electronic, optical, and thermoelectric properties and its pressure dependency for optoelectronic and thermoelectric applications. We follow the first principle calculation method us-

ing Density Functional Theory (DFT) as implemented in WIEN2k code. Density Functional Theory (DFT) is a computational method used in quantum mechanics to study the electronic structure of atoms, molecules, and solids. It simplifies calculations by focusing on electron density rather than directly solving complex equations, making it a valuable tool for predicting material properties, simulating chemical reactions, and advancing research in materials science and nanotechnology [37]. WIEN2k, a powerful software package developed by Peter Blaha and his team, utilizes the Full Potential Linearized Augmented Plane Wave (FP-LAPW) method within the framework of DFT [38]. Renowned for its accuracy, WIEN2k is versatile in studying various materials, from metals to insulators and magnetic substances. It plays a crucial role in investigating electronic and magnetic properties, predicting crystal structures, and unraveling complex phenomena in condensed matter physics and materials science. Together, DFT and WIEN2k form an effective combination, offering valuable insights into electronic behavior and advancing our understanding of diverse materials.

This project aims to provide a comprehensive analysis of structural, electronic, optical, and thermoelectric properties of $NaGeI_3$ under ambient and pressurized conditions. In this study, chapter 2 and 3 contains the background theories related to the calculations and density functional theory. In chapter 4, we discused the results we found for the compound both in ambient and pressurized conditions. In last chapter, we make a conclusion about the compound and its applicability as a practical device.

Chapter 2

Basic Quantum Mechanics

2.1 Schrödinger's equation

The Schrödinger equation one of the fundamental equations of quantum mechanics and describes the spatial and temporal behavior of quantum-mechanical system. The Schrödinger equation is a linear partial differential equation that governsthe wave function of a quantum-mechanical system [39]. Austrian physicist Erwin Schrödinger first proposed the equation in 1926 [40]. The Schrödinger equation can be time-dependent and time-independent. The time-independent Schrödinger equation is

$$\hat{H}\psi(\vec{r}) = \hat{E}\psi(\vec{r}). \tag{2.1}$$

where $\hat{H}$ is the hamiltonian, ψ is the wave function and $\hat{E}$ is the energy eigenvalue.

Using the Hamiltonian for a single particle

$$\hat{H} = \hat{T} + \hat{V} = -\frac{\hbar^2}{2m}\vec{\nabla}^2 + V(\vec{r}). \tag{2.2}$$

this equation leads to the time-independent single-particle Schrödinger equation

$$\hat{E}\psi(\vec{r}) = [-\frac{\hbar^2}{2m}\vec{\nabla}^2 + V(\vec{r})]\psi(\vec{r}). \tag{2.3}$$

For N particles in three dimensions, the Hamiltonian is

$$\hat{H} = \sum_{i=1}^{N} \frac{\hat{p}_i^2}{2m_i} + V(\vec{r}_1, \vec{r}_2, ..., \vec{r}_N). \tag{2.4}$$

The corresponding Schrödinger equation is

$$\hat{E}\psi(\vec{r}_1, \vec{r}_2, ..., \vec{r}_N) = [\sum_{i=1}^{N} \frac{\hat{p}_i^2}{2m_i} + V(\vec{r}_1, \vec{r}_2, ..., \vec{r}_N)]\psi(\vec{r}_1, \vec{r}_2, ..., \vec{r}_N). \tag{2.5}$$

2.1.1 The wave function

The wave function of a particle, at a particular time, contains all the information that anybody at that time can have about the particle (e.g.position, momentum and energy). The wave function can specify entirely the configuration or state of a quantum particle. It is not a real quantity, but a complex-valued functions of space and time. It has no physical interpretation and also not measurable, but the square of the wave function has a physical interpretation. In one dimension, the wave function is denoted by $\psi(x)$.

The wave equation, in general, is derived by solving Schrödinger equation. The square of the wave function gives the probability density, i.e.

$$|\psi|^2 = |\psi * \psi|^2. \tag{2.6}$$

The wave function ψ must be finite everywhere. If ψ is finite for aparticular point, that means an infinite larger probability of finding the particles at that point. The wave function must be single valued. If it has more than one value at any point, that means more than one value of probability of finding the particle at that point which is obviously improbable. The wave function must be continuous and have a continuous first derivative everywhere and its must be normalized. For the sake

of simplicity the discussion is restricted to the time-independent wave function. A question always arising with physical quantities is about possible interpretations as well as observations. The Born probability interpretation of the wave function, which is a major principle of the Copenhagen interpretation of quantum mechanics, provides a physical interpretation for the square of the wave function as a probability density [41].

$$P = |\psi(\vec{r}_1, \vec{r}_2, ..., \vec{r}_N)|^2 d\vec{r}_1 d\vec{r}_2, ..., d\vec{r}_N. \tag{2.7}$$

Equation (2.7) describes the probability that particles 1,2,...,N are located simultaneously in the corresponding volume element $d\vec{r_1}, d\vec{r_2}, ..., d\vec{r_N}$ [37]. What happens if the positions of two particles are exchanged, must be considered as well. Following merely logical reasoning, the overall probability density cannot depend on such an exchange,i.e.

$$|\psi(\vec{r}_1, \vec{r}_2, ..., \vec{r}_i, \vec{r}_j, ..., \vec{r}_N)|^2 = |\psi(\vec{r}_1, \vec{r}_2, ..., \vec{r}_j, \vec{r}_i, ..., \vec{r}_N)|^2. \tag{2.8}$$

There are only two possibilities for the behavior of the wave function during a particle interchange. The first one is a symmetrical wave function, which does not change due to such an interchange. This corresponds to bosons (particles with integer or zero spin) [42,43]. The other possibility is an anti-symmetrical wave function, where an exchange of two particles causes a sign change, which corresponds to fermions interest, which are fermions. The anti-symmetric fermion wave function leads to the Pauli principle, which states that no two electrons can occupy the same state, whereas state means the orbital and spin parts of the wave function [44] (the term spin coordinates will be discussed later in more detail). The anti-symmetry principle can be seen as the quantum-mechanical formalization of pauli's theoritical ideas in the description of spectra (e.g. alkaline doublets) [45]. Another consequence of the probability of finding a particle in a volume element, setting the full range of coordinates as volume element must result in a probability of one, i.e. all particles must be found somewhere in space. This corresponds to the normalization condition

for the wave function.

$$\int d\vec{r}_1 \int d\vec{r}_2 ... \int d\vec{r}_N |\psi(\vec{r}_1, \vec{r}_2, ..., \vec{r}_N)|^2 = 1. \tag{2.9}$$

Equation (2.9) also gives insight on the requirements a wave function must fulfill in order to be physical acceptable. Wave functions must be continuous over the full spatial range and square-integratable [46]. Calculating the expectation value of the relevant observable for that wave function [47]. For an observable $\mathrm{O}(\vec{r}_1, \vec{r}_2, ..., \vec{r}_N)$, this can be written as

$$O = \langle O \rangle = \int d\vec{r}_1 \int d\vec{r}_2 ... \int d\vec{r}_N \psi * (\vec{r}_1, \vec{r}_2, ..., \vec{r}_N) \left\langle \hat{O} \right\rangle \psi(\vec{r}_1, \vec{r}_2, ..., \vec{r}_N). \tag{2.10}$$

2.2 Born-Oppenheimer (BO) approximation

The Born-Oppenheimer approximation is the first of several approximations used to simplify the solution of the Schrödinger equation. It is one of the basic concepts underlying the description of the quantum states of molecules. It simplifies the general molecular problem by separating nuclear and elecrtonic motions.

The Hamiltonian of a many-body system consisting of nuclei and electrons can be written as

$$\begin{aligned} H_{tot} = -\sum_I \frac{\hbar^2}{2M_I} \nabla^2_{\vec{R}_I} - \sum_i \frac{\hbar^2}{2m_e} \nabla^2_{\vec{r}_i} + \frac{1}{2} \sum_{\substack{I,J \\ I \neq J}} \frac{Z_I Z_J e^2}{|\vec{R}_I - \vec{R}_J|} \\ + \frac{1}{2} \sum_{\substack{i,j \\ i \neq j}} \frac{e^2}{|\vec{r}_i - \vec{r}_j|} - \sum_{I,i} \frac{Z_I e^2}{|\vec{R}_I - \vec{r}_i|}. \end{aligned} \tag{2.11}$$

Where the indexes I,J run on nuclei, i and j on electrons, $\vec{R}_I$ and M_I are positions and masses of the nuclei, $\vec{r}_i$ and m_e of the electrons, Z_I the atomic number of nucleus I. The first term is the kinetic energy of the nuclei, the second term is the kinetic ebergy of the electrons, the third term is the potential energy of nucleus-nucleus Coulomb interaction, the fourth term is the potential energy of electron-electron Coulomb interaction and the last term represents the potential energy of nucleus-

electron Coulomb interaction [48]. Since the nuclei are much heavier than electrons, the nuclei move much slower than the electrons. Therefore we can separate the movement of nuclei and electrons. So, the electronic wave function depends upon only the nuclear position but does not depends upon their velocities. The total wave function can be written as

$$\Psi(\{\vec{R}_I\},\{\vec{r}_i\}) = \Theta(\{\vec{R}_I\})\phi(\{\vec{r}_i\};\{\vec{R}_I\}). \tag{2.12}$$

Where $\Theta(\{\vec{R}_I\})$ describe the nuclei and $\phi(\{\vec{r}_i\},\{\vec{R}_I\})$the electrons. So, we can write the Schrödinger equation into two separate equation.

$$H_e\phi(\{\vec{r}_i\};\{\vec{R}_I\}) = V(\{\vec{R}_I\})\phi(\{\vec{r}_i\};\{\vec{R}_I\}). \tag{2.13}$$

Where,

$$H_e = -\sum_i \frac{\hbar^2}{2m_e}\nabla^2_{\vec{r}_i} + \frac{1}{2}\sum_{\substack{I,J \\ I\neq J}} \frac{Z_I Z_J e^2}{|\vec{R}_I - \vec{R}_J|} + \frac{1}{2}\sum_{\substack{i,j \\ i\neq j}} \frac{e^2}{|\vec{r}_i - \vec{r}_j|} - \sum_{I,i} \frac{Z_I e^2}{|\vec{R}_I - \vec{r}_i|}. \tag{2.14}$$

and

$$\left[-\sum_I \frac{\hbar^2}{2M_I}\nabla^2_{\vec{R}_I} + V(\{\vec{R}_I\})\right]\Theta(\{\vec{R}_I\}) = E'\Theta(\{\vec{R}_i\}). \tag{2.15}$$

Equation (2.17) is the equation for the electronic problem with the nuclei positions fixed. The significance of the BO approximation is to separate the movement of electrons and nuclei.

2.3 The Hartree-Fock approach

In The spirit of the Born-Oppenheimer approximation, the electronic equation for molecules that depends parametrically on the nuclear co-ordinates is approximated using the Hartree-Fock method. Hartree-Fock method is a method of approximation for the determination of the wave function and the energy of a quantum many-body system in a schrödinger equation [49]. Suppose that, ψ is approximated as an antisymmetrized product of N orthonormal spin orbitals $\psi_i(\vec{x})$, each a product of a

spatial orbital $\phi_k(\vec{r})$ and a spin function $\sigma(s) = \alpha(s)$ or $\beta(s)$, the Slater determinant,

$$\phi_{HF} = (N!)^{-\frac{1}{2}} \begin{bmatrix} \psi_1(\vec{x}_1) & \psi_2(\vec{x}_1) & ... & \psi_N(\vec{x}_1) \\ \psi_1(\vec{x}_2) & \psi_2(\vec{x}_2) & ... & \psi_N(\vec{x}_2) \\ \vdots & \vdots & \ddots & \vdots \\ \psi_1(\vec{x}_N) & \psi_2(\vec{x}_N) & ... & \psi_N(\vec{x}_N) \end{bmatrix} = (N!)^{-\frac{1}{2}} det[\psi_1, \psi_2, ..., \psi_N]. \tag{2.16}$$

A general expression for the Hartree-Fock energy is obtained by uses of the Slater determinant.

$$E_{HF} = \langle \psi_{HF} | \hat{H} | \psi_{HF} \rangle = \sum_{i}^{N} H_i + \frac{1}{2} \sum_{i,j=1}^{N} (J_{ij} - K_{ij}). \tag{2.17}$$

Where, the first term corresponds to the kinetic energy and the nucleus-electron interacrtions. So, the single particle contribution of the Hamiltonian is written as,

$$H_i = \int \psi_i^*(\vec{x})[-\frac{1}{2}\nabla^2 + V(\vec{x})]\psi_i(\vec{x})d\vec{x}. \tag{2.18}$$

And the last term of equation(2.17) correspond electron-electron interactions. They are called Coulomb (J_{ij}) and exchange integral (K_{ij}). We can write this term in the following way,

$$J_{ij} = \int \int \psi_i(\vec{x}_1)\psi_i^*(\vec{x}_1)\frac{1}{r_{12}}\psi_j^*(\vec{x}_2)\psi_j(\vec{x}_2)d\vec{x}_1 d\vec{x}_2. \tag{2.19}$$

$$K_{ij} = \int \int \psi_i^*(\vec{x}_1)\psi_j(\vec{x}_1)\frac{1}{r_{12}}\psi_i(\vec{x}_2)\psi_j^*(\vec{x}_2)d\vec{x}_1 d\vec{x}_2. \tag{2.20}$$

These integrals are all real, and $J_{ij} \geq K_{ij} \geq 0$.

2.3.1 Limitations and failings of the Hatree-Fock approach

Atoms as well as molecules can have an even or odd number of electrons. If the number of electrons is even and all of them are located in double occupied spatial

orbitals ϕ_i, the compoubd is in a singlet state. Such systems are called closed-shell systems. Compounds with an odd number of electrons as well as compounds with single occupied orbitals, are called open-shell systems respectively. These two types of systems correspond to two different approaches of the Hatree-Fock method. In the restricted HF method (RHF), all electrons are considered to be paired in orbitals whereas in the unrestricted HF method (UHF) this limitation is lifted totally. It is also possible to describe open-shell systems with a RHF approach where only the single occupied orbitals are excluded, which is then called a restricted open-shell HF (ROHF) which is an approach closer to reality but also more complex and therefore less popular than UHF. There are also closed-shell systems which require the unrestricted approach in order to get proper results. For instance, the description of the dissociation of H_2 (i.e.) the behavior at large internuclear distance, where one electron must be located at one hydrogen atom. Therefore the choice of method is always a very important point in HF calculations. Kohn states several $M = p^5$ with $3 \leq p \leq 10$ parameters for an output with adequate accuracy in the investigations of the H_2 system. For a sytem with $N = 100$ electrons, the number of parameters rises to

$$M = p^{3N} = 3^{300} \quad to \quad 10^{300} \approx 10^{150} \quad to \quad 10^{300} \tag{2.21}$$

According to the equation (2.21), energy reduction would have to be done in a space with at least 10^{150} dimension, which is well above current computer capabilities. As a result, HF methods are limited to situations involving a modest number of electron ($N \approx 10$). This barrier commonly referred to as the exponential well because of the exponential component in (2.21) [50]. Since a many electron wave function cannot be described entirely by a single Slater determinant, the energy obtained by HF calculations is always larger than the exact ground state energy. The most accurate energy obtainable by HF methods is called the Hatree-Fock limit. The difference between E_{HF} and E_{exact} is called correlation energy and can be denoted as [51]

$$E_{corr}^{HF} = E_{min} - E_{HF}. \tag{2.22}$$

Chapter 3

Density Function Theory

3.1 The electron density

A general statement concerning the computation of observables has been presented in 2.1.1 about the wave function ψ. This section is about a quantity that is computed in a similar manner. The electron density (for N electrons) as the basic variable of density functional theory is defined as

$$n(\vec{r}) = N \sum_{s_1} \int d\vec{x}_2 ... \int d\vec{x}_N \psi^*(\vec{x}_1, \vec{x}_2, ..., \vec{x}_N)\psi(\vec{x}_1, \vec{x}_2, ..., \vec{x}_N) \tag{3.1}$$

Wchich is the basic variable of density function theory. If the spin coordinates are neglected, the electron density can even be expressed as measurable observable only dependent on spatial coordinates.

$$n(\vec{r}) = N \int d\vec{r}_2 ... \int d\vec{r}_N \psi * (\vec{r}_1, \vec{r}_2, ..., \vec{r}_N). \tag{3.2}$$

The total number of electrons can be obtained the electron density over the spatial variables, which can e.g. be measured by X-ray diffraction.

$$N = \int d\vec{r} n(\vec{r}). \tag{3.3}$$

3.2 Thomas-Fermi Model

The predecessor to DFT was the Thomas-Fermi (TF) model proposed by Thomas and Fermi in 1927. In this method, they used the electron density n(**r**) as the basic variable instead of the wave function. The total energy of a system in an external potential $V_{ect(\mathbf{r})}$ is written as a function of the non-interacting electron density $n(\mathbf{r})$ as:

$$E_{TF}[n(\mathbf{r})] = A_1 \int n(\mathbf{r})^{\frac{5}{3}} d\vec{r} + \int n(\mathbf{r}) V_{ect}(\mathbf{r}) d\mathbf{r} + \frac{1}{2} \iint \frac{n(\mathbf{r}) n(\mathbf{r'})}{|\mathbf{r} - \mathbf{r'}|} d\mathbf{r} d\mathbf{r'} \tag{3.4}$$

where the first term is the kinetic energy of the non-interacting electron in a homogeneous electron gas (HEG) with $A_1 = \frac{3}{10}(3\pi^2)^{\frac{2}{3}}$ in the atomic units. The free electron energy state

3.3 Hohenberg-Kohn Theorem

The formulation of density functional theory as an exact theory of many body system was the approach of Hohenberg and Kohn. As we all know, the ground state energy and ground state wave function can be determined by minimizing $|\psi|$ (energy functionals) for an electronic system described all the properties for ground state. This discription in this report is confined only for non degenerate ground state. The theory is based upon two theorems.

3.3.1 Theorem 1

Statement: The ground state energy E is a unique functional of the electron density.

$$E = E[n(r)] \tag{3.5}$$

Proof: We know that the ground state particle density is $n(\mathbf{r})$ for a system and $V_{ext}(r)$ is the external potential for the system. The proof is based on minimum energy principle. Suppose we have different two potential V_{ext} and V'_{ext}, which is different from each other by a constant but read to the same ground state density $n_o(r)$.For that we will get the different Hamiltonian H and H' and different ground state wave functions.

$$\hat{H}\psi = E_o\psi \tag{3.6}$$

$$\hat{H}'\psi' = E'_o\psi' \tag{3.7}$$

Since ψ' is not the ground state of $\hat{H}$. It follows that

$$E_o < \left\langle \psi' | \hat{H} | \psi' \right\rangle \tag{3.8}$$

$$< \left\langle \psi' | \hat{H} | \psi' \right\rangle + \left\langle \psi' | \hat{H} - \hat{H}' | \psi' \right\rangle \tag{3.9}$$

$$< E'_o + \int n_o(r)[V_{ext}(r) - V'_{ext}(r)]dr \tag{3.10}$$

Similarly,

$$E'_o < \left\langle \psi | \hat{H}' | \psi \right\rangle < E_o + \int n_o(r)[V'_{ext}(r) - V_{ext}(r)]dr \tag{3.11}$$

By adding equation 3.8 and 3.11 we get,

$$E_o + E'_o < E'_o + E_o \tag{3.12}$$

As the hamiltonian is fully known, except for a constant shift of energy, it says that the many body wavefunction for all state are determined. Therefore all the properties of the system are completely determined if and only if the ground state density is known.

3.3.2 Theorem 2

Statement: If the functional E[n(r)] is known, the exact ground state energy and density can be fully determined.

Proof: The Universal functional can be written as,

$$F[n(r)] \equiv \hat{T}[n(r)] + E_{int}[n(r)] \tag{3.13}$$

where,

$\hat{T}[n(r)]$ = kinetic energy

$E_{int}[n(r)]$ = interaction energy of the particles.

According to variational principle, the energy functional $E[\psi']$ is

$$E[\psi'] \equiv \left\langle \psi' | \hat{T} + \hat{V}_{int} + \hat{V}_{ext} | \psi' \right\rangle \tag{3.14}$$

When $\psi' = \psi_o$, it has a global minimum value with a constant that the totat number of particles are conserved. According to HK theorem 1 ψ' must correspond to the ground state whose particle density is $n'(r)$ and external potential is V'_{ext}. Then $E[\psi']$ is a functional of $n'(r)$. According to the variational principle,

$$E[\psi'] \equiv \left\langle \psi' | \hat{T} + \hat{V}_{int} + \hat{V}_{ext} | \psi' \right\rangle = E[n'(r)] \tag{3.15}$$

$$E[\psi'] \equiv \int n'(r) V'_{ext} dr + F[n'(r)] > E[\psi_o] = \int n(r) V_{ext} dr + F[n_o(r)] = E[n_o(r)] \tag{3.16}$$

Hence, Energy functional $E[n(r)] \equiv \int n(r) V_{ext} dr + F[n_o(r)]$ evaluats for the correct ground state density n_o is lower than the value of the function of any other density n(r). By minimizing the total energy functional with respect to the variations in the density n(r), one could find the exact ground state density and energy.

3.4 Kohn-Sham Equation

Hohenberg and Kohn framework is not very usefull yet in actual calculation. The second Kohenberg-Kohn theorem is the only possibility for the minimization of energy. An example of an iterative approachis the Hatree equation for self consistent

single particle [50,52]. The Hatree equation is clearly a wavefunction based equation and it is not directly related to Hohenberg and Kohn. Hatree's approximation says that every electron moves in an effective single particle potential of the form of ,

$$v_H(\vec{r}) = -\frac{Z}{|\vec{r}|} + \int \frac{n(\vec{r})}{|\vec{r} - \vec{r'}|} d\vec{r}. \tag{3.17}$$

where,

$-\frac{Z}{|\vec{r}|}$ = attractive coulomb potential of a nucleus with an atomic number Z.

$\int \frac{n(\vec{r})}{|\vec{r}-\vec{r'}|}$ = correspond to the potential caused by the mean electron density distribution $n(\vec{r})$.

$n(\vec{r})$ can be expressed in terms of the single particle wave function,

$$n(\vec{r}) = \sum_{j=1}^{M} |\phi_j|^2. \tag{3.18}$$

According to the Pauli exclusion principle,the sum of above equation runs over the lowest eigenvalues. For single particle. 3N-dimensional Schrödinger equation can be written as,

$$[-\frac{1}{2}\vec{\nabla}^2 + v_H(\vec{r})] \quad \phi_j(\vec{r}) = \epsilon_j \phi_j(\vec{r}) \quad j = 1, ..., N. \tag{3.19}$$

Therefore Khon and Sham investegated the DFT applied to a system of N non-interacting electron in an external potential. The expression for the energy of such a system is,

$$E_{v(\vec{r})}[n'(\vec{r})] \equiv \int v(\vec{r}) n'(\vec{r}) d\vec{r} + T_s[n'(\vec{r})] \geq E. \tag{3.20}$$

where,

$n'(\vec{r}) = v$ respectable density for non-interacting electrons

$T_s[n'(\vec{r})]$ = kinetic energy of the ground state of those non-interacting electron [50].

In case of non-interacting electron, the Euler-Lagrange equation [53] can be written

as,

$$\delta E_v[n'(\vec{r})] \equiv \int \delta n'(\vec{r})[v(\vec{r}) + \frac{\delta}{\delta n'(\vec{r})} T_s[n'(\vec{r})]|_{n'(\vec{r})=n(\vec{r})} - \epsilon] d\vec{r} = 0. \tag{3.21}$$

where,

$n'(\vec{r})$ = exact ground state density for the potential $v(\vec{r})$.

ϵ = the Lagrangian multiplier to ensure particle density conservation.

For such a system the total ground state energy and particle density can simply be writen as,

$$E = \sum_{j=1}^{N} \epsilon_j. \tag{3.22}$$

and

$$n(\vec{r}) = \sum_{j=1}^{N} |\phi_j(\vec{r})|^2. \tag{3.23}$$

For an interacting case the construction of Eular-Lagrange equation becomes.

$$\delta E_v[n'(\vec{r})] \equiv \int \delta n'(\vec{r})[v_{eff}(\vec{r}) + \frac{\delta}{\delta n'(\vec{r})} T_s[n'(\vec{r})]|_{n'(\vec{r})=n(\vec{r})} - \epsilon] d\vec{r} = 0. \tag{3.24}$$

with

$$v_{eff}(\vec{r}) \equiv v(\vec{r}) + \int \frac{n(\vec{r})}{|\vec{r} - \vec{r'}|} d\vec{r} + v_{xc}(\vec{r}). \tag{3.25}$$

and the functional derivative

$$v_{xc}(\vec{r}) \equiv \frac{\delta}{\delta n'(\vec{r})} E_{xc}[n'(\vec{r})]|_{n'(\vec{r})=n(\vec{r})}. \tag{3.26}$$

The corresponding equations are the single pafticle Schrödinger equation

$$[-\frac{1}{2}\vec{\nabla}^2 + v_{eff}(\vec{r})] \quad \phi_j(r) = \epsilon_j \phi_j(\vec{r}) \quad j = 1, ..., N. \tag{3.27}$$

As well as the equation for the particle density is

$$n(\vec{r}) = \sum_{j=1}^{N} |\phi_j(\vec{r})|^2. \tag{3.28}$$

Which form togather self consistent Khon-Sham equation and effective potential. If one use the exact $E_{xc}[n(\vec{r})]$ and $v_{xc}[n(\vec{r})]$ it would be possible to find the exact solution.

3.5 Solving Kohn-Sham euation

In a condensed matter system the KS equationgives a way to obtain the exact density and energy of the ground state. The process starts with an initial electron density $n(\vec{r})$, usually a superposition of atomic electron density, then the effective KS potential V_{KS} is calculated and the KS equation is solved with single-particle eigenvalues and wavefunctions, a new electron density is then calculated from the wavefunctions.

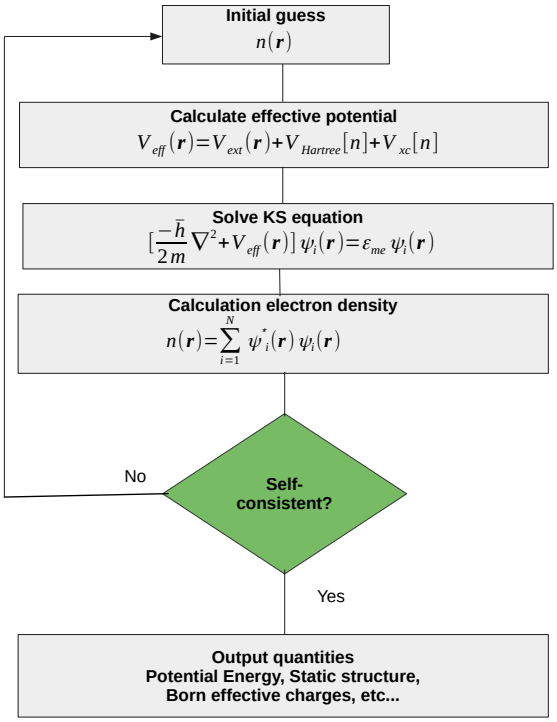

Figure 3.1: Flow chart of solving the Khon-Sham equation.

This is usually done numerically through some self consistent iteration as shown in above flowchart. Self-consistent condition(s) can be the change of total energy or electron density from the previous iteration or total force acting on atoms is less than some chosen small quantity, or a combonation of these individual conditions.

If the self-consistency is not achieved, the calculated electron density will be mixed with electron density from previous iterations to get a new electron density. A new iteration will start with the new electron density. This process continues until self-consistency is reached [54]. After the self-consistency is reached, various quantities can be calculated including total energy, force, stress, eigenvalues, electron density of states, band structure , etc..

3.6 The Exchange-correlation (XC) functional

The exchange correlation potential of the Khon-Sham density functional scheme is the difference between the fermi potential, an effective potential appears in the one electron Schrödinger equation for the equation for the square root of the electron density and Pauli potential , i.e. $v_{XC}(\mathbf{r}) = v_F(\mathbf{r}) - v_P(\mathbf{r})$ [55]. Generally, two approximation methods have been accomplished to approximate the exchange-correlation functional. The first approximation method of the exchange-correlation functional is the local density approximation (LDA). The Generalized gradient approximation (GGA) is the second approximation method in the Khon-Sham exchange-correlation function. In the generalized gradient approximation (GGA), the exchange and correlation energies include the local electron density and the local gradient in the electron density. The LDA is traditionally based on knowledge of the energy of the infinite three-dimensional (3D) homogeneous electron gas [56]. The XC energy per electron at a point $\vec{r}$ is considered the same as that for a homogeneous electron gas (HEC) that has the same electron density at the point $\vec{r}$. The total exchange-correlation functional $E_{XC}[n(\vec{r})]$ can be written as

$$E_{XC}^{LDA}[n(\vec{r})] = \int n(\vec{r})\epsilon_{XC}^{hom}(n(\vec{r}))d\vec{r} = E_X^{LDA}[n(\vec{r})] + E_C^{LDA}[n(\vec{r}). \tag{3.29}$$

The defination of the XC energy functional of GGA is the generalized form in equation(3.34) of LDA to include corrections from density gradient ($\vec{r}$) as

$$E_{XC}^{GGA}[n(\vec{r})] = \int n(\vec{r})\epsilon_{XC}^{hom}(n(\vec{r}), |(\vec{r})|, ...)d\vec{r}. \tag{3.30}$$

Where ϵ_{XC}^{hom} is the exchange energy density of HEG. GGA generally works better than LDA, in predicting bond length and ninding energy of molecules, crystal lattiec constants, and so on, especially systems where the charge density is rapidly varying [57].

Chapter 4

Results and discussion

4.1 Computational details

In this work, lead-free halide peroveskite $NaGeI_3$ has been investigated using full potential linear augmented plane wave (FP-LAPW) method, as implemented in the WIEN2k code based on density functional theory (DFT). To find the optimized ground states of the considered materials, the generalized gradient approximation (GGA) with the Perdew-Burke-Ernzerhof (PBE) approximation was used. The exchange correlation potential was solved by generalized gradient approximation (GGA) that underestimates the band gap value. the later needed to be corrected using Tran-Blaha modified Becke and Johnson local density approximation (TB-mBJ) methods provide accurate results in good agreement for optical properties and band gap with experimental data. The basic functions are expended into spherical harmonic function inside the muffin-tin sphere and Furier series in the interstitial region. The value of RK_{max} was set to 7, where K_{max} is the plane wave cut-off and R_{MT} is the smallest of all atomic sphere radii. The energy convergence criteria was set to 10^{-5}Ry, while the charge convergence criteria was also set to $10^{-4}e$, where e is an electron charge and the number of k-points in the Brillouin zone is approximately 10^4. Finally, the BoltzTraP code was employed under an approximation of constant

relaxation time for the thermoelectric properties evaluation.

4.2 Crystallographic Structure

The crystal structure of halide perovskite $NaGeI_3$ is a cubic structure with a space-group of ($pm\bar{3}m$) (space group number 221). The estimated crystallographic structure are depicted in Figure 4.1. The lattice constant for the structure is 5.91 Å. The Wyckoff positions of Na, Ge and I atoms are as follows: Na (0.0, 0.0, 0.0), Ge (0.5, 0.5, 0.5) and I (0.0, 0.5, 0.5). The volume optimization is provided with WIEN2k package that determines the minimum energy possessed by a system by plotting volume as a function of energy, which has been shown in Figure 4.2.

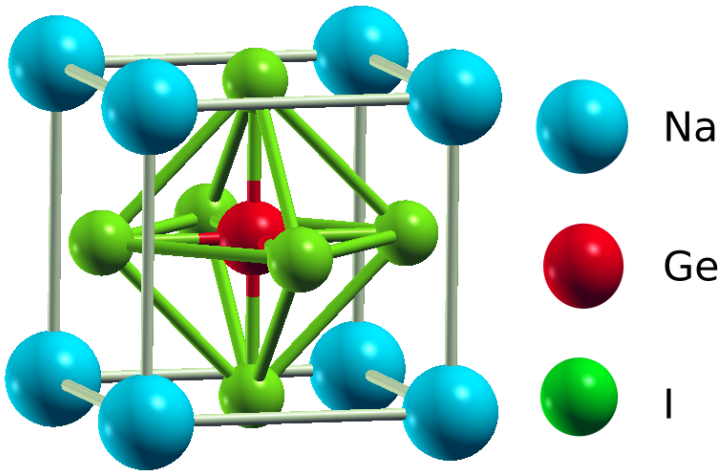

Figure 4.1: Ball and stick structure of cubic perovskite halide $NaGeI_3$.

In order to determine the optimized ground states of the materials being studied, the energy versus volume of a unit cell of the crystals was calculated. The Birch-Murnaghan thermodynamic state relation is used as the basis for this analysis. The lattice constant of $NaGeI_3$ perovskite has been found to be 5.91 Å and this value decreases when pressure increases, which is shown in Table 4.1.

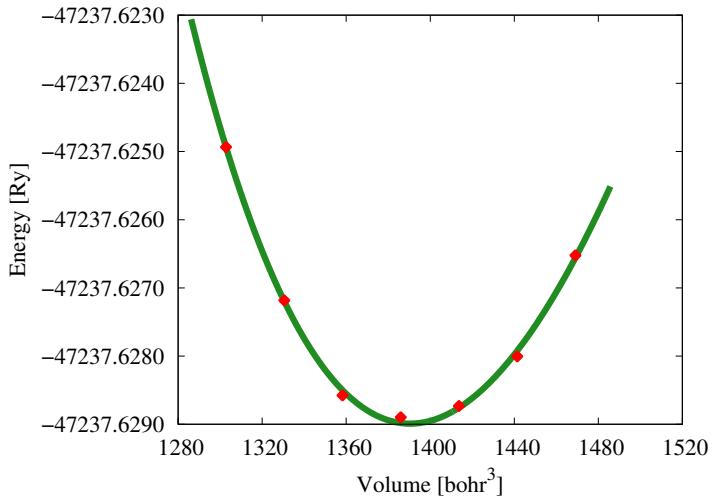

Figure 4.2: Energy versus volume optimization curves of $NaGeI_3$.

Table 4.1: Calculated lattice parameters (Å) and band structure of $NaGeI_3$ at different hydrostatic pressure.

Pressures (GPa)	Lattice parameters (Å)	Band gap (eV)
0	5.91	0.49
1	5.81	0.35
2	5.75	0.17
3	5.68	0.03
4	5.64	0.00

4.3 Electronic Properties

The electronic properties are predominanntly resolved taking into account the high symmetry direction of the Brillouin zone (BZ). The study of electronic properties is crucial to gain a clear concept about optical properties of $NaGeI_3$ alloy. The basic electronic properties including band structure, density of states (DOS), and charge density. TB-mBJ potential is used to calculate the electronic properties under hydrostatic pressure ranging from 0 to 4 GPa.

4.3.1 Band structure

The electronic band structure is a representation of the allowed electronic energy levels of materials and is used to better inform their electrical properties. The estimated band structures are depicted in Figure 4.3. The black horizontal dashed line at 0 eV indicates the Fermi level, which denoted by (E_F), whereas the valance band (VB) and conduction band (CB) are presented by colored lines below and above the E_F, respectively. In this study, the energy band is considered from -4 to $+4$ eV. $NaGeI_3$ has a direct band gap (E_g) of 0.49 eV at R point of the Brillouin zone at ambient pressure. The conduction band minima at R point begin to move towards the E_F are illustrated in Figure 4.3, resulting in a lowering of E_g. The valance band maxima and conduction band minima at 4 GPa for $NaGeI_3$. E_g vanishes, exhibiting that $NaGeI_3$ transforms from semiconducting to conducting nature.

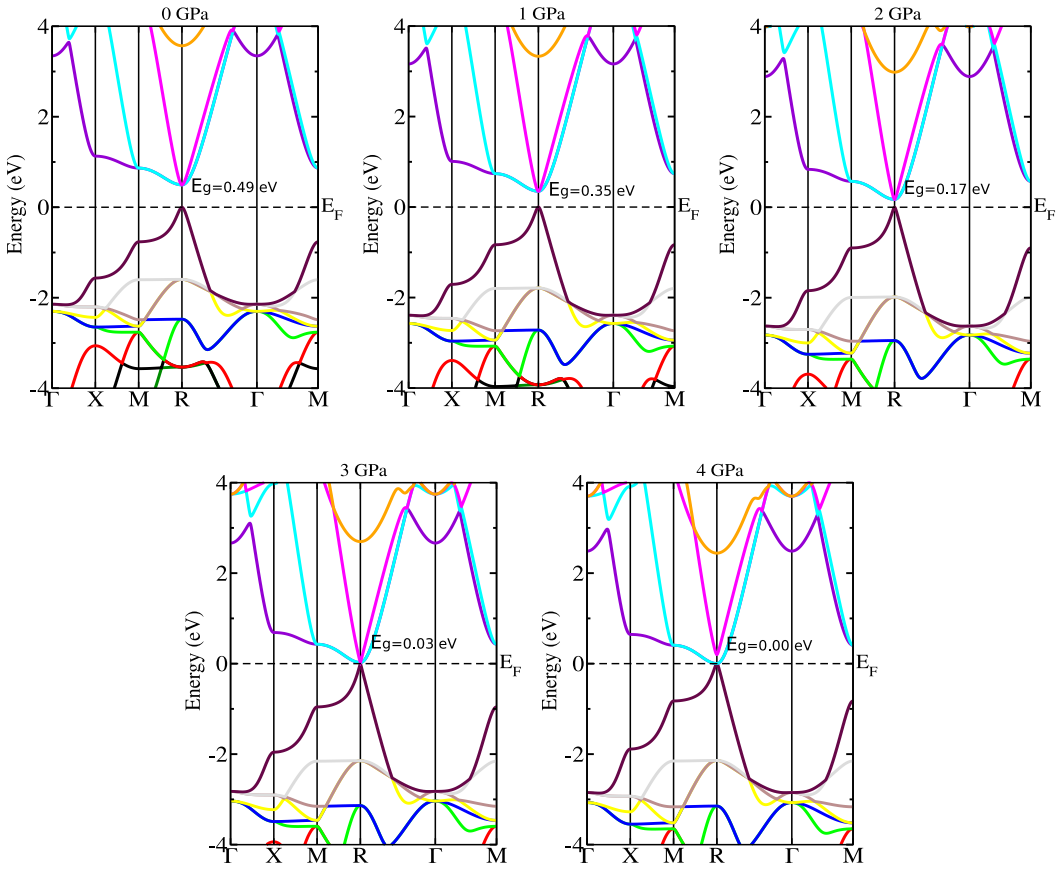

Figure 4.3: The calculated band structures of $NaGeI_3$ under various applied pressures.

4.3.2 Density of states

The density of states (DOS) is essentialy the number of different states at a particular energy level that electrons are allowed to occupy, i.e. the number of electron states per unit volume per unit energy. DOS also describes the electronic states contribution toward valance and conduction bands and accurately interprets the size of band gap. To demonstrate the electronic behavior, the calculated partial density of states (PDOS) of $NaGeI_3$ under various pressure is depicted in Figure 4.5(a,b). The black dashed vertical line at 0 eV also reprasent the Fermi level. The valance band of the system is dominated by I-5p for $NaGeI_3$ with Ge-4p states. However, if the pressure increased continuously the contribution of I-5p state also reduces. In this case, there is no contribution of Na-3s state. The conduction band originated from the contributions of Ge-4p state of $NaGeI_3$, in which the contribution of Ge-4p is higher than those of other orbitals. At 4 GPa the conduction and valence bands collapse at Fermi level and diminishes the band gap. As a consequence, the electronic nature shifts from semiconductor to metallic nature with increase in pressure. On the contrary, the total density of states (TDOS) of $NaGeI_3$ under pressure is presented in Figure 4.4(a). It also observed that the nonzero value of TDOS appeared at the Fermi level, when pressure is 4 GPa of $NaGeI_3$.

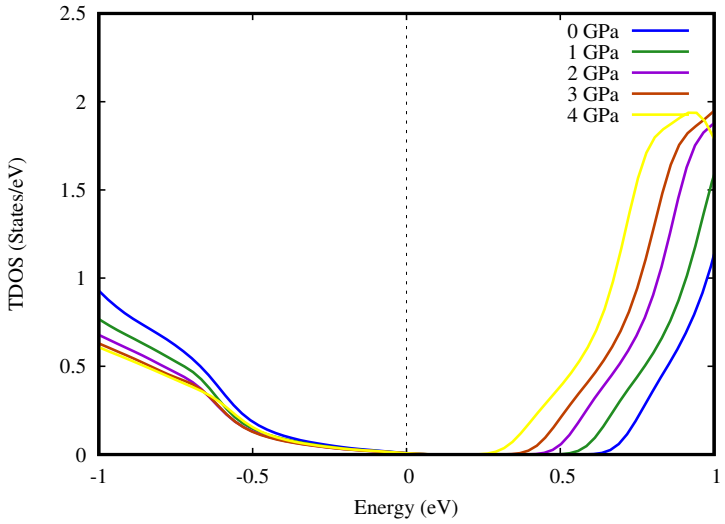

Figure 4.4: The total density of states of cubic perovskite $NaGeI_3$ under pressure.

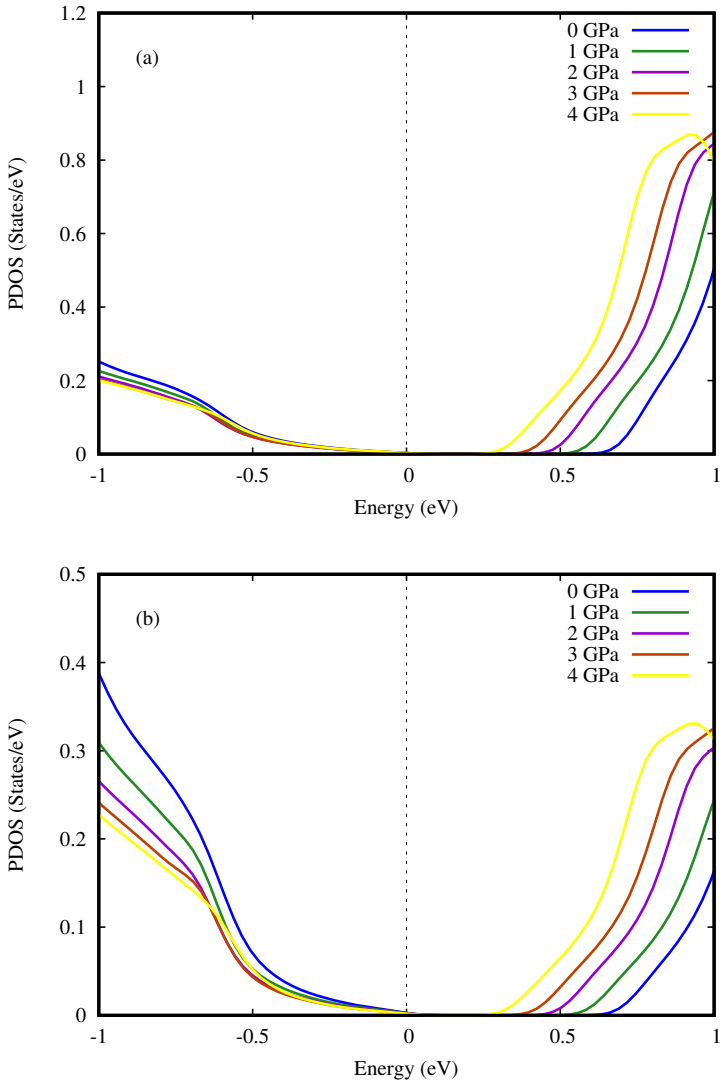

Figure 4.5: The total density of states (a) and partial density of states (b) of cubic perovskite $NaGeI_3$ under pressure.

4.4 Electron density

Charge density is the measure of electric charge per unit area of a surface, or per unit volume of a body or field, which describes how much charge is stored in a particular field. To obtain clear concept about the chemical bonding in $NaGeI_3$, Figure 4.6 illustrate the charge density along the crystallographic planes (101) and (100) at 0, 1, 2 and Figure 4.7 depicts those of at 3 and 4 GPa pressure. At 0 GPa, the charge distributions of Na and I atoms do not overlap along the (100) and (100) planes, which indicates ionic bond of those atoms. But a few overlapping of Ge and I atoms along the (101) plane, exposing the covalent bonding of Ge-I. However,

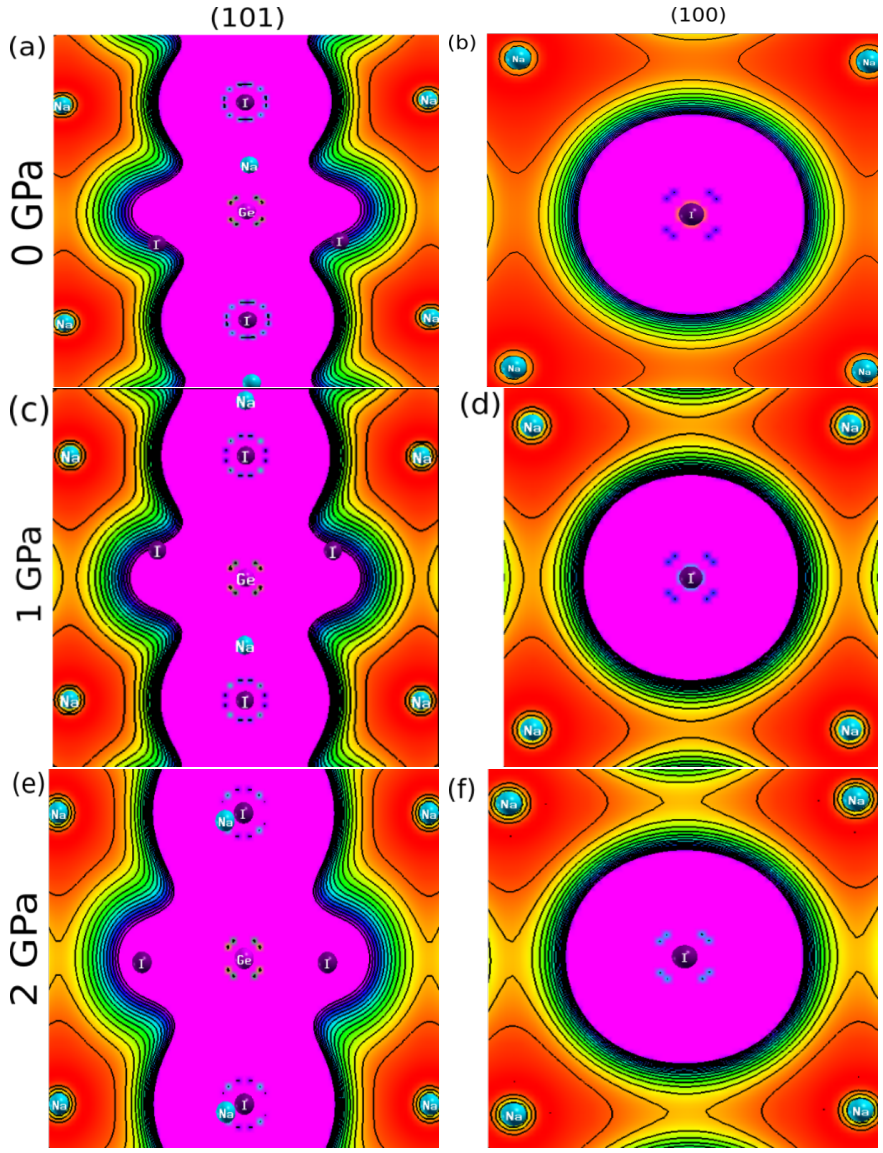

Figure 4.6: The calculated electron density of $NaGeI_3$ (a,c,e) for (101) plane and (b,d,f) for (100) plane at 0, 1, and 2 GPa pressure respectively.

the space between Na and I reduces along the (100) plane without overlaping the charge distribution while pressure rises, preserving the ionic nature of Na-I bond. The overlaping between Ge and I atoms increases more along the (101) plane under pressure, also representing the covalent nature of Ge-I bond.

4.5 Optical properties

Optical properties define how it interacts with light. To understand the optical properties of perovskite halid $NaGeI_3$, we need to studied the dielectric function, absorp-

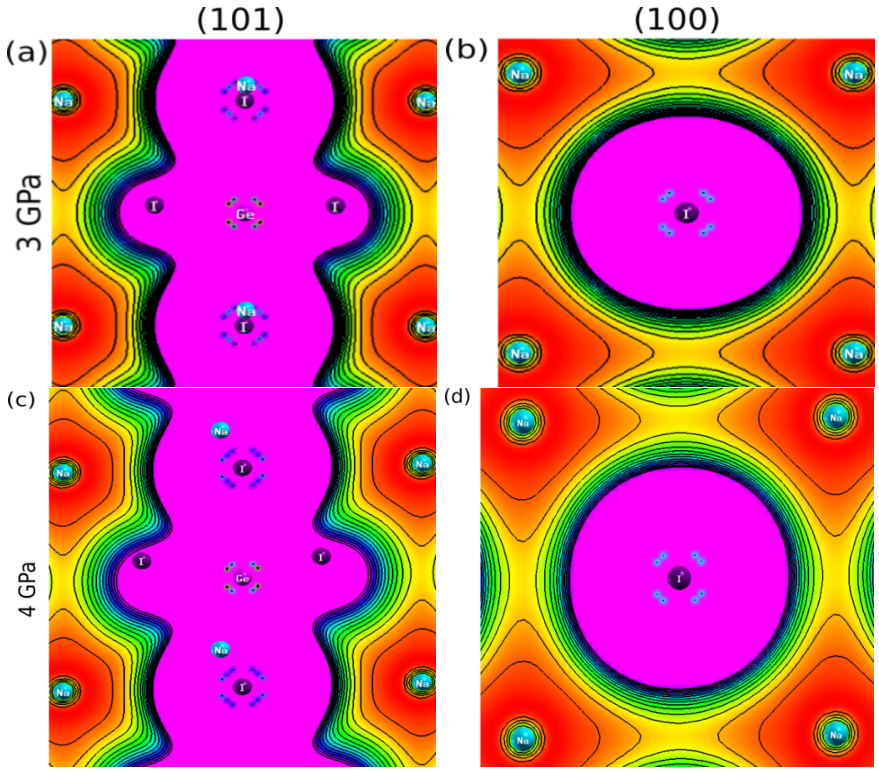

Figure 4.7: The calculated electron density of $NaGeI_3$ (a,c) for (101) plane and (b,d) for (100) plane at 3 and 4 GPa pressure respectively.

tion coefficient, conductivity, reflectivity and refractive index etc. These properties are investigated under various hydrostatic pressures up to 4 GPa. We have calculate all this properties through MBJ-LDA potential functional.

4.5.1 Dielectric function

The dielectric function is one important optical properties of $NaGeI_3$, which mainly consists of two parts such as real dielectric function and imaginary dielectric function. The dielectric function is denoted by the symbol $\epsilon(\omega)$. It is defined as

$$\epsilon(\omega) = \epsilon_1(\omega) + i\epsilon_2(\omega). \tag{4.1}$$

To determine the real dielectric function, the transformation of Kramers-Kronig is implemented and the components of the momentum matrix are used to calculate the imaginary dielectric part [58]. The real part of $NaGeI_3$ dielectric permittivity is depicted in Figure 4.8(a) for photon energies up to 12 ev. The real component of the dielectric function can be used to learn about the polarization and dispersion

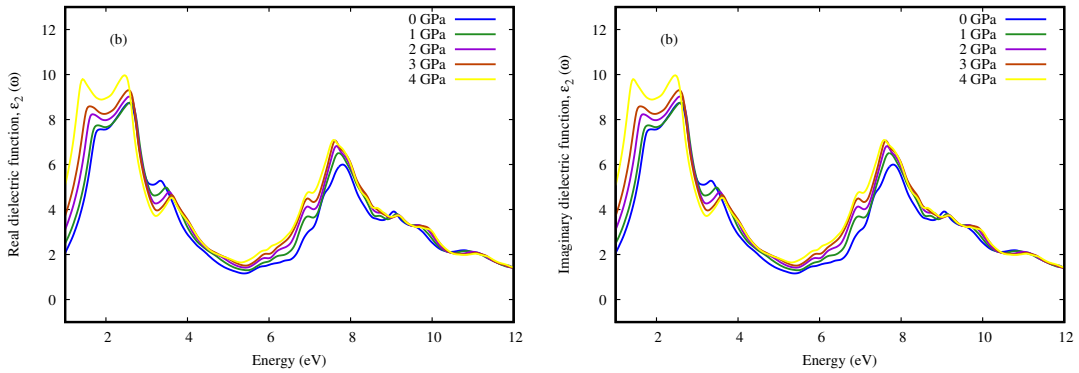

Figure 4.8: (a) Real dielectric function and (b) imaginary dielectric function of cubic $NaGeI_3$ as a function of energy under various applied pressures.

impacts. The maximum frequency of Zero, denoted as $\epsilon(0)$, which refers to the electronic component of the real state of the function.On the contorary,the charactristics of the dielectric function's imaginary part is illustrated in Figure 4.8(b). The imaginary function plays an important role in the analysis of optical absorption and the crystal structure's energy storage potential.

4.5.2 Optical conductivity

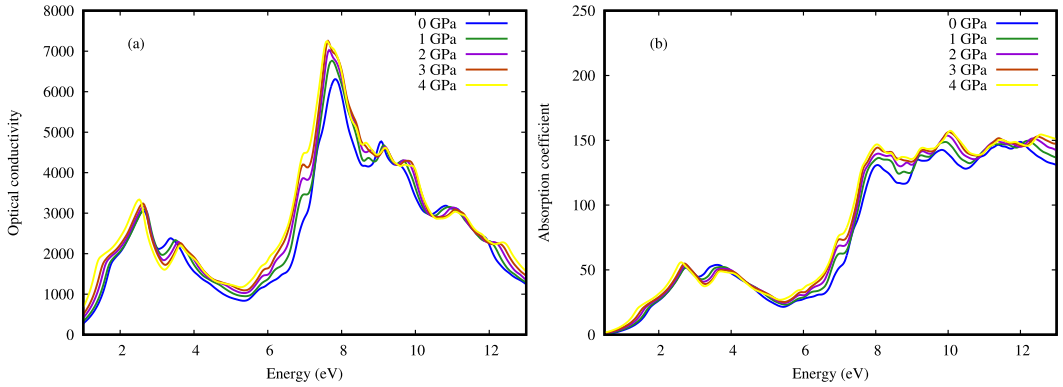

Figure 4.9: (a) Optical conductivity and (b) Absorption coefficient of cubic $NaGeI_3$ as a function of energy under various applied pressures.

Optical conductivity is the property of a material which interprets the relation between the induced current density in the material and the magnitued of the including electric field for arbitrarily selected frequencies. In Figure 4.9(a) is illustrated the optical conductivity as a function of energy. From the curve, it is observed that the maximum conductivity peaks are obtained at 8 eV under various pressure and from the energy point optical conductivity continuesly decreases as energy increase and

also reaches zero for higher energy values.

4.5.3 Absorption coefficient

The absorption coefficient is mainly used to determine how far into a material light of a particular wavelength can penetrate before it is absorbed. When a material has low absorption coefficient, light is absorbed poorly and vice-versa. It depends on the material and also on the wavelength of light which is being absorbed. In Figure 4.9(b) represents the absorption coefficient of $NaGeI_3$ alloy. The attenuation of light of a particular energy into a material is predicted by optical absorption coefficient of the material. From Figure 4.9(b) also depict, the absorption peaks become more sharper with high pressure such as 4 GPa.

4.5.4 Refractive index

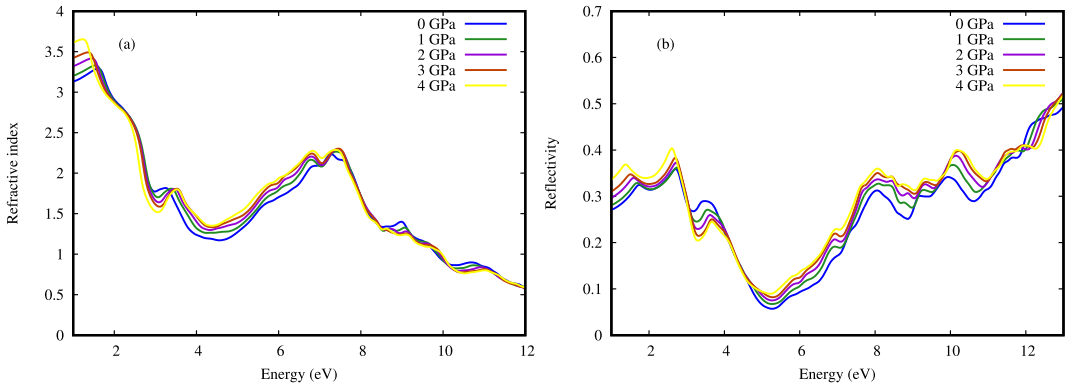

Figure 4.10: (a) Refractive index and (b) Optical reflectivity of cubic $NaGeI_3$ as a function of energy under various applied pressures.

Refractive index of a material, also called index of refraction, which measures how much path of light is bent when it enters that material. Since refractive indices are inversely related to the bandgap, so the bandgap decreases as the refractive index increases. The refractive index vs energy curve is illustrated in Figure 4.10(a), in which the maximum peak of the refractive index appears at 2 eV and rises an incremental application of hydrostatic pressure. It also infrom the energy value index of refraction decreases and finally reaches zero at higher energies.

4.5.5 Optical reflectivity

Reflectivity is another most important optical property of material measured while light is incident on the surface of the material. The optical reflectivity plots represent that reflectivity increases with energy after 5.5 eV. when pressure increased reflectivity also rises.It also show the reflectivity spcetrum being minimum in the infrared and visible regions. From Figure 4.10(b), it also obivious that the maximum reflectivity in the vacuum UV region at higher energies. The high optical reflectivity represents the strong metallic characteristic of the $NaGeI_3$ compound.

4.6 Thermoelectric characteristics

BoltzTraP computational code was used to predict the thermoelectric characteristics of $NaGeI_3$ alloy. To shorten environmental pollution and to avoid energy disasters, thermoelectric materials are of great interest, transforming wasted heat into useful electricity [59, 60]. Thermoelectric parameters, including electrical conductivity (σ/τ) and thermal conductivity (κ/τ) as well as figure of merit (ZT) and Seebeck coefficient (S), were calculated for $NaGeI_3$. The mobility of charge carries have been estimated in terms of the electrical conductivity (σ/τ), which was plotted in the temperature range 100-1000 K, as depict in Figure 4.11(a). The magnitude of σ/τ for $NaGeI_3$ is increased with pressure, which indicates $NaGeI_3$ is semiconductor. At 4 GPa pressure, the perovskite material $NaGeI_3$ shows (σ/τ) higher conductivity. This conductivity also increased linearly with the increased of temperature, which also proved the semiconducting nature of the materials. Another part of the conductivity comes from lattice vibration and thermal agitation, which is called thermal conductivity (κ/τ), and that is illustrated in Figure 4.11(b). Thermally agitated lattice vibrations create phonon waves. The rate of increase of κ/τ is faster than σ/τ with temperature. The increases in the value of κ/τ with temperature indicates that at a higher temperature more lattice vibrations are generated, which causes an increase in κ/τ [60]. Since the value of κ/τ for $NaGeI_3$ is of the order of 10^{14}, this reveals the suitability of this composition for thermoelectric device applications.

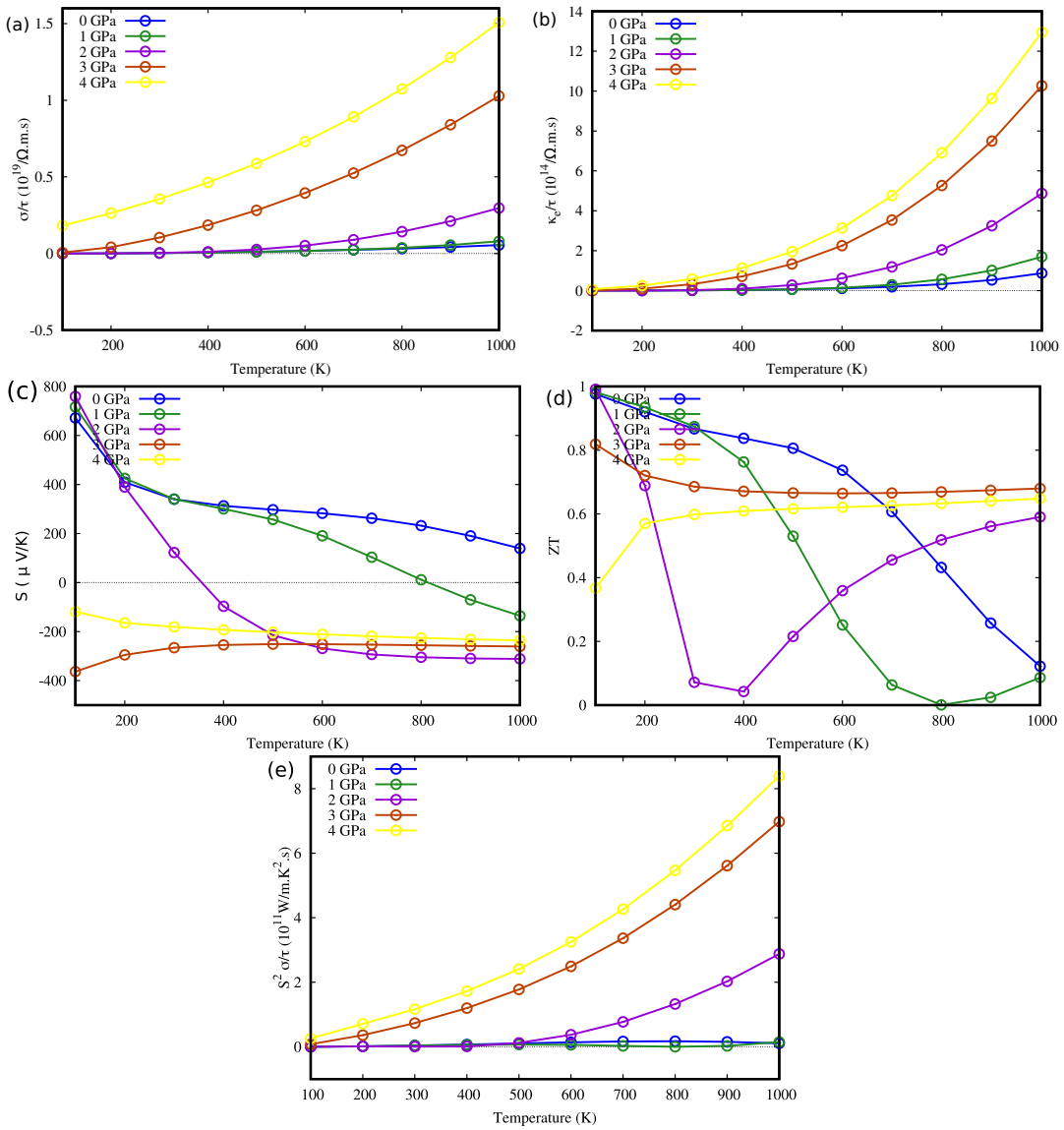

Figure 4.11: The calculated thermoelectric properties of $NaGeI_3$ (a) electrical conductivity (σ/τ), (b) thermal conductivity (κ/τ), (c) Seebeck coefficient (S), (d) figure of merit (ZT) and (e) power factor (PF) under various applied pressures.

The Seebeck coefficient (S) is used to find the potential difference that can occur between the contacts of dissimilar metals as a function of temperature change, which is shown in Figure 4.11(c). The positive values of S for $NaGeI_3$ indicates that positive charge carriers are the majority charge carriers of the material. The seebeck coefficient increases with temperature, but at high temperature it decreases due to the presence of thermally excited minority carriers. From Figure 4.11(c) depict that the value of S reduces with the incremental applications of pressure. The power factor (PF) is another important thermoelectric parameter that is used to determine the thermoelectric performance of any materials and this is calculated by

the expression PF $=\sigma S^2$. The temperature dependent variation of PF is depict in Figure 4.11(e). As the temperature increases, the power factor (PF) at all pressures increase and reach the maximum value at 1000 K.

Another important factor to estimate the actual thermoelectric efficiency of the studied compound, a dimensionless parameter labeled as figure of merit i.e., ZT $= (\sigma S^2/$ K) was used to assess their thermoelectric performance. The parameters σ, S, and K represents electrical conductivity, Seebeck coefficient and thermal conductivity, respectively. The variation of ZT for the $NaGeI_3$ perovskite halid in the temperature range 100-1000 K under several pressure, which is illustrate in Figure 4.11(d). For $NaGeI_3$, the value of figure of merit decreases with temperature under pressure except 4 GPa. At different hydrostatic pressure, $NaGeI_3$ alloy shows that with pressure the value of ZT also increases, but at 2 GPa the perovskite material $NaGeI_3$ shows some different behavior that pressure first ZT decreases with temperature but at 400 K it increases continuously with temperature up to 1000 K. This pressure shows some different nature for $NaGeI_3$ alloy.

Chapter 5

Conclusions

The structural, electronic, optical, and thermoelectric properties of Ge-based halide $NaGeI_3$ perovskite have been investigated using the WIEN2k package within the framework of DFT under various hydrostatic pressures to enhance our understanding of the systems and evaluate the impact of pressure. The corresponding lattice parameters of $NaGeI_3$ at ambient pressure are 5.91 Å. The observed direct energy band gap is 0.46 eV, calculated by the PBE-GGA functional, and 0.49 eV, calculated by the TB-mBJ functional. The material's band gap reduces with incremental pressure, leading to a metallic transition from its semiconducting nature. The computed density of states reveals the energy band gap. The charge density aids in understanding the chemical bonding in $NaGeI_3$, maintaining ionic and covalent bonds Na-I and Ge-I, respectively. Pressure induction significantly increases the optical conductivity and optical absorption of $NaGeI_3$, making it suitable for optoelectronic devices. The computed thermoelectric properties under hydrostatic pressure, using the BoltzTraP code, reveal that as pressure rises, electrical conductivity, thermal conductivity, and power factor increase, while the Seebeck coefficient and figure of merit decrease. In conclusion, this study elucidates the pressure-induced transformations in $NaGeI_3$ perovskite, unveiling its potential for optoelectronic applications with enhanced structural, electronic, and optical properties.

Bibliography

[1] Tze-Zhang Ang, Mohamed Salem, Mohamad Kamarol, Himadry Shekhar Das, Mohammad Alhuyi Nazari, and Natarajan Prabaharan. A comprehensive study of renewable energy sources: Classifications, challenges and suggestions. *Energy Strategy Rev.*, 43:100939, 2022.

[2] Krishna Kumar Jaiswal, Chandrama Roy Chowdhury, Deepti Yadav, Ravikant Verma, Swapnamoy Dutta, Km Smriti Jaiswal, SangmeshB, and Karthik Selva Kumar Karuppasamy. Renewable and sustainable clean energy development and impact on social, economic, and environmental health. *Energy Nexus*, 7:100118, 2022.

[3] Gregory Soon How Thien, Kah-Yoong Chan, Ab Rahman Marlinda, Mohd Arif Mohd Sarjidan, Wan Haliza Abd Majid, and Boon Kar Yap. Active polymer-based halide perovskites for light-driven applications: A review. *Appl. Surf. Sci.*, 19:100538, 2024.

[4] Isabel Mesquita, Luísa Andrade, and Adélio Mendes. Perovskite solar cells: Materials, configurations and stability. *Renew. Sust. Energ. Rev.*, 82, 2017.

[5] Dibyajyoti Saikia, Atanu Betal, Jayanta Bera, and Satyajit Sahu. Progress and challenges of halide perovskite-based solar cell- a brief review. *Mater. Sci. Semicond.*, 150:106953, 2022.

[6] Priyanka Roy, Aritra Ghosh, Fraser Barclay, Ayush Khare, and Erdem Cuce. Perovskite solar cells: A review of the recent advances. *Coatings*, 12, 2022.

[7] Teddy Salim, Shuangyong Sun, Yuichiro Abe, Anurag Krishna, Andrew C. Grimsdale, and Yeng Ming Lam. Perovskite-based solar cells: impact of mor-

phology and device architecture on device performance. *J. Mater. Chem. A*, 3:8943–8969, 2015.

[8] Mohammad Ismail Hossain, Ahmed M. Saleque, Safayet Ahmed, Ilhom Saidjafarzoda, Md. Shahiduzzaman, Wayesh Qarony, Dietmar Knipp, Necmi Biyikli, and Yuen Hong Tsang. Perovskite/perovskite planar tandem solar cells: A comprehensive guideline for reaching energy conversion efficiency beyond 30%. *Nano Energy*, 79:105400, 2021.

[9] Tanishq Dureja, Anirudh Garg, Sirjan Bhalla, Divya Bhutani, and Arrik Khanna. Double lead-free perovskite solar cell for 19.9% conversion efficiency: A SCAPS-1D based simulation study. *Mater. Today: Proc.*, 71:239–242, 2022.

[10] Yangying Zhou, Xuewen Yin, Qi Zhang, Ning Wang, Atsushi Yamamoto, Kunihito Koumoto, and Heping Shen. Perovskite solar cell-thermoelectric tandem system with a high efficiency of over 23%. *Mater. Today Energy*, 12, 04 2019.

[11] Zhelu Hu, Chenxin Ran, Hui Zhang, Lingfeng Chao, Yonghua Chen, and Wei Huang. The current status and development trend of perovskite solar cells. *Engineering*, 21:15–19, 2023.

[12] T. Ibn-Mohammed, S.C.L. Koh, I.M. Reaney, A. Acquaye, G. Schileo, K.B. Mustapha, and R. Greenough. Perovskite solar cells: An integrated hybrid lifecycle assessment and review in comparison with other photovoltaic technologies. *Renew. Sust. Energ. Rev.*, 80:1321–1344, 2017.

[13] Juan-Pablo Correa-Baena, Antonio Abate, Michael Saliba, Wolfgang Tress, Jesper Jacobsson, Michael Graetzel, and Anders Hagfeldt. The rapid evolution of highly efficient perovskite solar cells. *Energy Environ. Sci.*, 10, 2017.

[14] Yingzhuang Ma and Qing Zhao. A strategic review on processing routes towards scalable fabrication of perovskite solar cells. *J. Energy Chem.*, 64:538–560, 2022.

[15] Evan D. Jacque, Richard A. Korneisel, Konstantinos Gerasopoulos, and Michael H. C. Jin. Scalable, solution-based dye-sensitized photovoltaic fibers with an electrolytic solid-state ion conductor. *Sol. Energy*, 264:111999, 2023.

[16] Bin Ding, Lili Gao, Lusheng Liang, Qianqian Chu, Xiaoxuan Song, Yan Li, Guan-Jun Yang, Bin Fan, Mingkui Wang, Cheng-Xin Li, and Chang-Jiu Li.

Facile and scalable fabrication of highly efficient lead iodide perovskite thin-film solar cells in air using gas pump method. *ACS Appl. Mater. Interfaces*, 8, 2016.

[17] Baohua Wang, Xudong Xiao, and Tao Chen. Perovskite photovoltaics: A high-efficiency newcomer to solar cell family. *Nanoscale*, 6, 2014.

[18] Boucar Diouf, Aarti Muley, and Ramchandra Pode. Issues, challenges, and future perspectives of perovskites for energy conversion applications. *Energies*, 16, 2023.

[19] Ju Yang, Dong In Kim, Rak Jeong, Seong Park, and Jin-Hyo Boo. Enhancement of perovskite solar cell performance by external down-conversion of Eu-complex film. *Int. J. Energy Res.*, 46, 2022.

[20] Sarah Brittman, Gede Adhyaksa, and Erik Garnett. The expanding world of hybrid perovskites: Materials properties and emerging applications. *MRS Commun.*, 5:1–20, 2015.

[21] Zhe Shi, Rasoul Kh, Massoud Malaki, and Han Zhang. Mxene-based materials for solar cell applications. *Nanomater.*, 11:3170, 2021.

[22] Pankaj P. Khirade and Anil V. Raut. Perovskite structured materials: Synthesis, structure, physical properties and applications. *Intech*, 2022.

[23] Haizhou Lu, Anurag Krishna, Shaik Zakeeruddin, Michael Grätzel, and Anders Hagfeldt. Compositional and interface engineering of organic-inorganic lead halide perovskite solar cells. *iScience*, 2020.

[24] Michael Lee, Joël Teuscher, Tsutomu Miyasaka, Takurou Murakami, and Jeong-Hyeok Im. Efficient hybrid solar cells based on meso-superstructured organometal halide perovskites. *Science (New York, N.Y.)*, 338, 2012.

[25] Rabia Sharif, Arshi Khalid, Syed Waqas Ahmad, Abdul Rehman, Haji Ghulam Qutab, Hafiz Husnain Akhtar, Khalid Mahmood, Shabana Afzal, and Faisal Saleem. A comprehensive review of the current progresses and material advances in perovskite solar cells. *Nanoscale Adv.*, 5:3803–3833, 2023.

[26] Mohammad Abdur Rashid, Md Saiduzzaman, Arpon Biswas, and Khandaker Hossain. First-principles calculations to explore the metallic behavior of semi-

conducting lead-free halide perovskites $RbSnX_3$ (X = Cl, Br) under pressure. *Eur. Phys. J. Plus*, 13:649, 2022.

[27] Md Borhanul Asfia, Sahadat Jaman, and Mohammad Abdur Rashid. Pressure induced band gap shifting from ultra-violet to visible region of $RbSrCl_3$ perovskite. *Mater. Res. Express*, 9:095902, 2022.

[28] Mei Li, Tianbiao Liu, Yonggang Wang, Wenge Yang, and Xujie Lü. Pressure responses of halide perovskites with various compositions, dimensionalities, and morphologies. *Matter Radiat. Extrem.*, 5:018201, 2020.

[29] Long Zhang, Kai Wang, Yu Lin, and Bo Zou. Pressure effects on the electronic and optical properties in low-dimensional metal halide perovskites. *J. Phys. Chem. Lett.*, 2020.

[30] Md. Shoriful Islam, Md. Ferdous Rahman, Md. Rasidul Islam, Avijit Ghosh, Md. Abdul Monnaf, Md. Selim Reza, M. Khalid Hossain, Abid Zaman, Safa Ezzine, and Lamia Ben Farhat. An in-depth analysis of how strain impacts the electronic, optical, and output performance of the Ca_3NI_3 novel inorganic halide perovskite. *J. Phys. Chem. Solids.*, 185:111791, 2024.

[31] Long Zhang, Qingxin Zeng, and Kai Wang. Pressure-induced structural and optical properties of inorganic halide perovskite $CsPbBr_3$. *J. Phys. Chem. Lett.*, 8, 2017.

[32] Ovijit Das, Md Saiduzzaman, Khandaker Monower Hossain, Ismile Khan Shuvo, Mohammad Mizanur Rahman, Sohail Ahmad, and S.K. Mitro. First-principles calculations to investigate pressure-driven electronic phase transition of lead-free halide perovskites $KMCl_3$ (M = Ge, Sn) for superior optoelectronic performance. *Results Phys.*, 44:106212, 2023.

[33] N.A. Noor, Muhammad Rashid, Ghulam M. Mustafa, M.I. Khan, Asif Mahmood, and Shahid M. Ramay. Study of pressure induced physical properties of $ZnZrO_3$ perovskite using density functional theory. *Chem. Phys. Lett.*, 753:137601, 2020.

[34] Lei Zhang and Shuai Lin. Dimensional tailoring of halide perovskite: A case study on $Cs_4PbBr_6/CsPbBr_3$ hybrid with molecular halide perovskite. *Sol. Energy Mater Sol. Cells.*, 204:110237, 2020.

[35] Kamal Hossain, Rabeya Akter Rabu, Mst Shamima Khanom, Md Kamal Hossain, and Farid Ahmed. First-principles study of structural, mechanical, lattice dynamics, superconducting and optoelectronic properties of the $Pd_3Pb_2Se_2$ shandite under hydrostatic pressure. *Phys. B: Condens.*, 637:413920, 2022.

[36] A.G. Asadov, D.P. Kozlenko, A. Mammadov, R. Mehdiyeva, S.E. Kichanov, E.V. Lukin, O.N. Lis, and A.V. Rutkauskas. A structural phase transition in $La_2Ti_2O_7$ at high pressure. *Phys. B: Condens.*, 655:414753, 2023.

[37] Niklas Zwettler. Density functional theory. *University of Graz.*

[38] Fabien Tran Robert Laskowski Georg K. H Madsen Peter Blaha, Karlheinz Schwarz and Laurence D. Marks. WIEN2k: An APW+lo program for calculating the properties of solids. *J. Chem. Phys.*, 152:074101, 2020.

[39] David J Griffiths and Darrell F Schroeter. Introduction to quantum mechanics. *Cambridge university press*, 2018.

[40] E Schrodinger. Schrodinger 1926e. *Ann. Phys.*, 81:109, 1926.

[41] Max Born. Quantenmechanik der stoßvorgange. *Z. phys.*, 38(11):803–827, 1926.

[42] Wolfgang Pauli. The connection between spin and statistics. *Phys. Review*, 58(8):716, 1940.

[43] Arthur Jabs. Connecting spin and statistics in quantum mechanics. *Found. Phys.*, 40(7):776–792, 2010.

[44] Attila Szabo and Neil S Ostlund. Modern quantum chemistry: introduction to advanced electronic structure theory. *Courier Corporation*, 2012.

[45] Wolfgang Pauli. On the connexion between the completion of electron groups in an atom with the complex structure of spectra. *Z. Phys.*, 31:765, 1925.

[46] Nouredine Zettili. Quantum mechanics: concepts and applications. *Wiley-VCH*, 2003.

[47] Klaus Capelle. A bird's-eye view of density functional theory. *Braz. J. Phys.*, 36:1318–1343, 2006.

[48] M. Born and R. Oppenheimer. Zur quantentheorie der molekeln. *Ann. Phys.*, 84:457–484, 1927.

[49] Christian B Lang and Norbert Pucker. Mathematische methoden in der physik. *Springer*, 2, 2005.

[50] W. Kohn. Electronic structure of matter-wave functions and density functionals. *Rev. Mod. Phys.*, 71:1253–1266, 1999.

[51] Per-Olov Lowdin. Scaling problem, virial theorem, and connected relations in quantum mechanics. *J. Mol. Spectrosc.*, 3(1-6):46–66, 1959.

[52] D.R. Hartree. The wave mechanics of an atom with a non-coulomb central field. part i. theory and methods. *Math. Proc. Cambridge Philos.*, 24:89–110, 1928.

[53] T. Flieÿbach. Mechanik: Lehrbuch zur theoretischen physik i (german). *Spektrum*, 2009.

[54] Rüdiger Bauernschmitt and Reinhart Ahlrichs. Stability analysis for solutions of the closed shell kohn–sham equation. *J. Chem. Phys.*, 104(22):9047–9052, 1996.

[55] Viktor N. Staroverov and Egor Ospadov. Unified construction of fermi, pauli and exchange-correlation potentials. *Academic Press*, 79, 2019.

[56] Carl-Olof Almbladh and Robert van Leeuwen. Variational total energies from ϕ-and ψ-derivable theories. *Int. J. Mod. Phys.*, 13, 1999.

[57] John P. Perdew, Kieron Burke, and Matthias Ernzerhof. Generalized gradient approximation made simple. *Phys. Rev. Lett.*, 78:1396–1396, 1997.

[58] Avijit Ghosh, Md. Ferdous Rahman, and Md. Rasidul Islam. Structural, electronic and optical characteristics of inorganic cubic perovskite Sr_3AsI_3. *Opt. Continuum*, 2:2144–2153, 2023.

[59] Yingzhi Zhou, Jing Wang, Dongxiang Luo, Dehua Hu, Yonggang Min, and Xue Qifan. Recent progress of halide perovskites for thermoelectric application. *Nano Energy*, 94:106949, 2022.

[60] Sile Hu, Zhilin Ren, Aleksandra Djurišić, and Andrey Rogach. Metal halide perovskites as emerging thermoelectric materials. *ACS Energy Lett.*, 6:3882–3905, 2021.